Published in final edited form as:

Cell Rep. 2016 September 20; 16(12): 3157–3166. doi:10.1016/j.celrep.2016.08.046.

Increased Persistent Sodium Current Causes Neuronal Hyperexcitability in the Entorhinal Cortex of *Fmr1* Knockout mice

Pan-Yue Deng and **Vitaly A. Klyachko**[#]

Departments of Cell Biology and Physiology, Biomedical Engineering, Washington University School of Medicine, St. Louis, MO 63110

SUMMARY

Altered neuronal excitability is one of the hallmarks of fragile X syndrome (FXS), but the mechanisms underlying this critical neuronal dysfunction are poorly understood. Here we find that pyramidal cells in the entorhinal cortex of *Fmr1* KO mice, an established FXS mouse model, display a decreased AP threshold and increased neuronal excitability. The AP threshold changes in *Fmr1* KO mice are caused by increased persistent sodium current (I_{NaP}). Our results indicate that this abnormal I_{NaP} in *Fmr1* KO animals is mediated by increased mGluR5-PLC-PKC signaling. These findings identify Na^+ channel dysregulation as a major cause of neuronal hyperexcitability in cortical FXS neurons and uncover a mechanism by which abnormal mGluR5 signaling causes neuronal hyperexcitability in a FXS mouse model.

Graphical abstract

[#]Corresponding author and lead author: klyachko@wustl.edu, Tel: (314) 362-5517, Fax: (314) 362-7463.

Additional details are available in Supplemental Experimental Procedures.

AUTHOR CONTRIBUTIONS

P.Y.D. and V.A.K. conceived and designed the study. P.Y.D. conducted the experiments, and analyzed the data. P.Y.D. and V.A.K. wrote the manuscript.

The authors declare no competing financial interests.

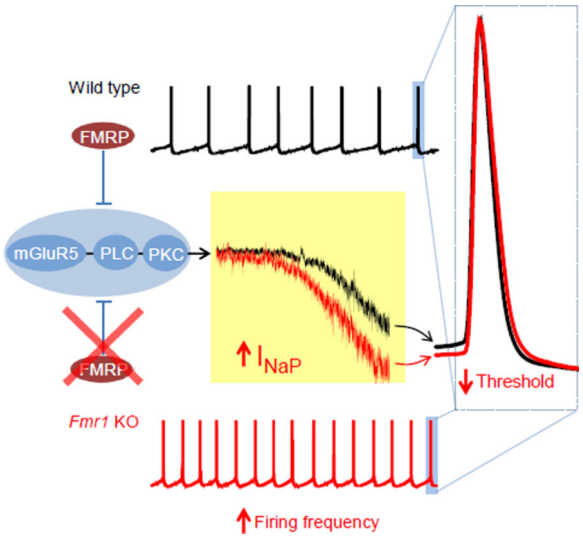

INTRODUCTION

Fragile X syndrome (FXS), the most common cause of inherited intellectual disability, is typically associated with cognitive, behavioral and social impairments, as well as a wide range of neurological abnormalities (Santoro et al., 2012). A prominent characteristic of neurological defects in FXS is neuronal hyperexcitability, which is believed to cause a variety of symptoms, including hyperactivity, increased sensitivity to sensory stimuli, and a high incidence of seizures (Contractor et al., 2015). These phenotypes account for a considerable part of the disease pathophysiology. However, the underlying mechanisms responsible for increased neuronal excitability in FXS remain poorly understood.

Altered neuronal excitability has been reported in various brain regions of FXS models (Deng et al., 2013; Gibson et al., 2008; Kalmbach et al., 2015; Myrick et al., 2015; Tang and Alger, 2015; Zhang et al., 2014). Among these regions, the parahippocampal cortices, and particularly the entorhinal cortex (EC), play an essential role in generation and maintenance of a wide range of seizure syndromes (Chatzikonstantinou, 2014). Anatomically, EC mediates the majority of connections between various brain regions and the hippocampus, which is one of the most heavily investigated brain areas implicated in the pathology of FXS (Santoro et al., 2012). The EC is thus regarded as the gateway to the hippocampus and has been implicated as one of the key epileptogenic brain areas (Chatzikonstantinou, 2014). Despite its critical role in cortico-hippocampal network excitability, little is known about pathophysiological changes in the EC that occur in FXS models. EC thus represents a highly relevant model system to investigate excitability defects in FXS.

Action potential (AP) threshold is one of the key determinants of neuronal excitability (Bean, 2007). The threshold determines when an AP is initiated, sets the neuron's firing rate and shape neuronal computations, including coincidence detection, temporal coding and feature selectivity (Bean, 2007). AP threshold is governed predominately by Na^+ channel availability and activation propensity near the threshold, whereas K^+ channels and other conductances can dynamically modulate AP threshold in an adaptive way (Carter and Bean,

2009; Hu et al., 2009; Platkiewicz and Brette, 2010). In addition to the fast transient Na^+ current (I_{NaT}) underlying AP rising phase, the Na^+ channels can give rise to a noninactivating persistent Na^+ current (I_{NaP}) that activates at subthreshold voltages (Crill, 1996). Although the amplitude of I_{NaP} is generally small relative to the I_{NaT}, it is highly functionally significant and may strongly influence transduction of synaptic inputs into AP generation (Crill, 1996; Hu et al., 2009). Here we demonstrate that I_{NaP} is abnormally increased in the EC layer III excitatory pyramidal neurons of *Fmr1* KO mice, leading to decreased AP threshold and increased neuronal excitability. Our results suggest that this enhanced I_{NaP} is caused by exaggerated mGluR5 signaling acting via phospholipase C (PLC) and protein kinase C (PKC), a signaling mechanism distinct from the well-established mGluR5 signaling cascade affecting local translation in *Fmr1* KO animals. These findings identify Na^+ channel dysregulation as a major cause of neuronal hyperexcitability in cortical FXS neurons and uncover a previously unrecognized mechanism by which abnormal mGluR5 causes neuronal hyperexcitability in an FXS mouse model. Our findings may thus provide a therapeutic strategy to ameliorate neuronal excitability defects in FXS.

RESULTS

Increased Pyramidal Cell Excitability in the Entorhinal Cortex of *Fmr1* KO Mice

Superficial layers (layers II–III) of the EC serve as an information gateway to the hippocampus. Accordingly, we first asked whether the excitability of the principal neurons in EC superficial layers (i.e., layer II stellate cells and layer III pyramidal cells (PCs)) is altered in *Fmr1* KO mice. APs were evoked by a ramp current injection (Yamada-Hanff and Bean, 2013) (Figure 1A). Only the first APs were used to determine AP threshold to avoid the effect of ramp current cumulatively inactivating Na^+ channels on the threshold of following APs (Figure 1A,B). No changes in AP threshold was observed in the stellate cells of *Fmr1* KO mice (WT −36.50 ± 0.56 mV, n = 7; KO −36.65 ± 0.69 mV, n = 11, p = 0.517, Figure 1C). In contrast, we found that the threshold potential of layer III PCs had a significant hyperpolarizing shift in *Fmr1* KO mice (WT −38.31 ± 0.82 mV, n = 6; KO −41.88 ± 0.33 mV, n = 6, p = 0.0096; Figure 1C).

We further examined the excitability of EC layer III PCs by setting the resting membrane potential at −51 mV through automatic current injection to induce AP firing spontaneously. At this membrane potential, about 70% of WT neurons and all tested *Fmr1* KO neurons fired spontaneously (data not shown). Our results confirmed the increased excitability of these neurons in *Fmr1* KO mice, as evident by the increased mean firing frequency (WT 3.75 ± 0.70 Hz, n = 23; KO 6.12 ± 0.52 Hz, n = 48, p=0.0082; Figure 1D,E,F) and decreased AP threshold (WT −39.93 ± 0.33 mV; KO −42.61 ± 0.21 mV, p<0.00001; Figure 1G). We further verified the increased excitability of *Fmr1* KO neurons by examining the distribution of instantaneous AP firing frequency in the tested neurons (Figure 1E). Specifically, we noted that in *Fmr1* KO neurons the first peak of firing frequency shifted from 2.3 to 3.9 Hz, and an additional 3rd peak appeared at ~15 Hz (Figure 1E). We therefore used the layer III PCs as a model to elucidate the underlying mechanisms of this defect.

Abnormal Persistent Na^+ Current Causes Increased Excitability in EC Layer III Pyramidal Cells of *Fmr1* KO Mice

Because the intrinsic membrane properties play a major role in setting neuronal excitability, we compared the resting membrane potential (RMP), input resistance and membrane capacitance in EC layer III PCs of *Fmr1* KO and WT animals, but found no significant differences in any of these parameters between genotypes (Figure S1A-C). We further found that changes in tonic excitatory/inhibitory inputs do not account for the increased excitability of EC Layer III PCs in *Fmr1* KO mice (Figure S2). In fact, we noted that sIPSC frequency was increased in *Fmr1* KO neurons (Figure S2B) suggesting a compensatory action of tonic inhibition. However, this effect of tonic inhibition was insufficient to counter-balance the increased excitability of Layer III PCs in *Fmr1* KO mice since our observations of decreased AP threshold and increased firing in these neurons were made in the intact EC circuits (Figure 1D-G), in the presence of this compensatory effect of tonic inhibition.

Since sub-threshold currents are believed to have critical role in controlling RMP and regulating AP initiation and thus setting neuronal excitability, we then probed whether changes in sub-threshold currents play a role in the increased excitability in *Fmr1* KO neurons. There are 3 major types of sub-threshold currents in central neurons: M current (I_M, carried by Kv7 channels), H current (I_h, carried by HCN channels) and I_{NaP} (Honigsperger et al., 2015; Stafstrom, 2007; Yamada-Hanff and Bean, 2013, 2015). We thus used specific inhibitors of I_M, I_h or I_{NaP} to probe their role in regulating neuronal excitability in EC Layer III PCs. The Kv7 channel inhibitor XE991 (10 μM) had no detectable effect on RMP (Figure $2A_1$), suggesting a low activity of these channels at the potentials around RMP in EC Layer III PCs. XE991 slightly decreased the threshold potential in both WT and *Fmr1* KO neurons, but it failed to affect the differences in threshold between genotypes (XE991: WT −40.02 ± 0.71 mV, n=7; KO −44.01 ± 1.25 mV, n=6, p=0.0051; Figure $2A_2$). Unlike XE991, the HCN channel blocker ZD7288 (10 μM) markedly hyperpolarized the RMP both in WT and *Fmr1* KO neurons to the same extend (ZD7288: WT −79.20 ± 0.73, n=6; KO −79.83 ± 1.80 mV, n=6; p=0.769; Figure $2B_1$), suggesting a high activity of HCN channels at the potentials around RMP in both genotypes. However, ZD7288 failed to abolish the difference in AP threshold between genotypes (ZD7288: WT −37.63 ± 0.97 mV; KO −43.69 ± 0.66 mV; p=0.00047; Figure $2B_2$). Finally, low concentration of TTX (20 nM) to block I_{NaP} (Hammarstrom and Gage, 1998) had a small, but significant hyperpolarizing effect on RMP in both genotypes (Basal: WT −66.45 ± 0.78 mV, n=11; KO −66.12 ± 1.11 mV, n=7, p=0.816; TTX: WT −70.0 ± 0.89 mV; KO −68.57± 1.13 mV, p=0.336; Basal vs. TTX within genotype: WT p=0.0014; KO p=0.0023; Figure $2C_1$). Most importantly, TTX (20 nM) abolished the difference in AP threshold between genotypes (WT −29.75 ± 0.87 mV; KO −31.75 ± 1.48 mV; p=0.239; Figure $2C_2$). These results point to abnormal I_{NaP}, but not I_M or I_h, as a potential cause of the decreased AP threshold in *Fmr1* KO neurons.

Increased Persistent Sodium Current Underlies AP Threshold Changes in *Fmr1* KO Mice

To verify the above observations and examine changes in I_{NaP} in *Fmr1* KO neurons, we recorded I_{NaP} evoked by a slow depolarization ramp (20 mV/s) to measure its quasi-steady-state voltage dependence (Yamada-Hanff and Bean, 2015), using the same internal and external solutions as those used above in AP recordings. The TTX-sensitive current was first

evident at ~ −65 mV (Figure 3A). AP currents that escaped voltage clamp control were present in most neurons. As expected, I_{NaP} was significantly increased in *Fmr1* KO neurons (I_{NaP} at −40 mV: WT −1.88 ± 0.55 pA/pF, n=5; KO −3.71 ± 0.52 pA/pF, n=5; p=0.0297; Figure 3B), while the voltage-dependent activation of I_{NaP} was not altered in *Fmr1* KO neurons (I_{NaP} half activation voltage $V_{1/2}$: WT −41.1 ± 0.33 mV, n=5; KO −40.7 ± 0.19 mV, n=5; p=0.5638; Figure 3C).

To further confirm these observations, we modified our protocol to avoid generation of escaped AP currents, and achieve more reliable I_{NaP} recordings. We also modified our recording solutions to include blockers of K^+ and Ca^{2+} channels to minimize contamination of I_{NaP} measurements from Na^+-activated K^+ currents and other K^+ and Ca^{2+} conductances. Briefly, we used a Cs^+-based internal solution supplemented with 4-AP (2 mM) and TEA (10 mM), and also included TEA (20 mM, to replace equimolar NaCl) and $CdCl_2$ (100 μM) in external solution. Under these conditions and using a repolarizing ramp voltage (+30 to −65 mV, −50mV/s) to evoked I_{NaP}, we could record I_{NaP} without any AP currents out of voltage clamp control. In these measurements we focused on the voltage in the range from −65 to −20 mV for better comparison with the above results. It is noteworthy that, within a certain voltage range, activation of I_{NaP} has been shown to be independent of polarity of the voltage ramp (Astman et al., 2006). Indeed, consistent with the findings above, we found that I_{NaP} was significantly larger in *Fmr1* KO than WT neurons (I_{NaP} at −40mV: WT −1.29 ± 0.23 pA/pF, n=7; KO −2.21 ± 0.32 pA/pF, n=6; p=0.0066 Figure $3D_{1,2}$). As in experiments above, the voltage-dependent activation of I_{NaP} was not different between genotypes ($V_{1/2}$: WT −36.27 ± 0.28 mV; KO −36.49 ± 0.41 mV, p=0.9738; Figure $3D_3$). We note that the half activation voltage $V_{1/2}$ was shifted to a more depolarizing voltage in both genotypes compared to the above measurements (Figure 3C), presumably due to the changes in internal/external solutions (Na^+ and K^+ gradients, K^+ and Ca^{2+} channel blockers). Finally, using a potent I_{NaP} inhibitor riluzole (10 μM) (Spadoni et al., 2002; Urbani and Belluzzi, 2000), we further verified that the observed differences between *Fmr1* KO and WT are due to altered I_{NaP}. Indeed, riluzole (10 μM) eliminated differences in ramp-evoked current between genotypes (in riluzole at −40mV: WT −0.83 ± 0.16 pA/pF, n=6; KO −1.06 ± 0.24 pA/pF, n=6; p=0.195; Figure $3E_{1,2}$). Together, these results suggest that I_{NaP} is abnormally increased in *Fmr1* KO neurons. Our measurements further indicate that within the voltage range used in our recordings depolarizing and repolarizing ramp measurements of I_{NaP} are largely equivalent. Therefore, to avoid contamination from escaped AP currents, in the following experiments we will use the repolarizing ramps to record I_{NaP}.

If reduced AP threshold in *Fmr1* KO neurons results from increased I_{NaP}, then inhibition of I_{NaP} should abolish the differences in threshold between genotypes. Indeed, we found that riluzole (10 μM) abolished the difference in AP threshold between genotypes (WT −36.41 ± 2.15 mV, n=6; KO −37.38 ± 0.96, n=6; p=0.710; Figure $3E_3$). Moreover, we also found that the I_{NaP} opener veratridine (1 μM) shifted the threshold to a more hyperpolarizing voltages in both genotypes, and most importantly it also abolished the difference in AP threshold between genotypes (WT −44.36 ± 0.98 mV, n=6; KO −44.98 ± 0.45, n=6; p=0.613; Figure $3E_3$). The evidence that both I_{NaP} inhibitor riluzole and I_{NaP} opener veratridine abolished the difference in threshold between genotypes suggests that the abnormal I_{NaP} is unlikely caused by altered expression of Na^+ channels in *Fmr1* KO

neurons. Taken together, these results suggest that an abnormally enhanced I_{NaP} causes the increased excitability of EC layer III PCs in *Fmr1* KO mice.

Hyperexcitability of EC Layer III PCs in *Fmr1* KO Mice Is Mediated by Exaggerated mGluR5 Signaling

Na^+ channel activity is continuously and extensively modulated by a variety of signaling pathways, including metabotropic neurotransmitter receptors. Given a number of studies implicating dysfunction of mGluR5 or $GABA_BR$ signaling pathways in FXS models (Bear et al., 2004; Pacey et al., 2009; Wahlstrom-Helgren and Klyachko, 2015), both of which are known to modulate Na^+ channel properties (Crill, 1996), we examined whether these signaling pathways play a role in the changes of AP threshold in *Fmr1* KO neurons. We first pharmacologically isolated the cells from glutamatergic and GABAergic transmission networks by using a cocktail containing both fast and slow synaptic transmission blockers (in μM: 50 APV, 10 DNQX, 5 gabazine, 2 CGP55845 and 10 MPEP to block NMDA, AMPA, $GABA_A$, $GABA_B$ and mGluR5 receptors, respectively). Surprisingly, the cocktail of these 5 blockers completely abolished the difference in AP threshold between genotypes (WT −41.82 ± 0.15 mV, n = 6; KO −42.01 ± 0.17 mV, n = 7, p = 0.462; Figure 4A), indicating that changes in AP threshold in *Fmr1* KO neurons are mediated by activation of one or several signaling pathways coupled to these receptors. In line with our findings above that increased excitability could not be attributed to network changes in fast synaptic transmission, we found that inhibition of fast synaptic transmission alone (with APV, DNQX, and gabazine) failed to abolish the difference in threshold between genotypes (WT −41.75 ± 0.48 mV, n = 12; KO −43.71 ± 0.49 mV, n = 13, p = 0.0079; Figure 4A), pointing to abnormal metabotropic signaling pathways as mediators of AP threshold changes in *Fmr1* KO neurons. We further found that inhibition of $GABA_B$ receptors with CGP55845 in combination with fast transmission blockers, shifted the threshold in a hyperpolarizing direction for both genotypes, but more importantly, it failed to reduce differences in threshold between genotypes (WT −43.10 ± 0.69 mV, n = 6; KO −46.21 ± 0.61 mV, n = 6, p = 0.032; Figure 4A). In contrast, the mGluR5 blocker MPEP in combination with the fast transmission blockers abolished differences in AP threshold between genotypes (WT −41.43 ± 0.53 mV, n = 7; KO −42.11 ± 0.50 mV, n = 6, p = 0.914; Figure 4A). These results single out the dysfunction of mGluR5 signaling as a mediator of AP threshold defect in EC Layer III PCs in *Fmr1* KO mice. To verify this finding, we used another specific mGluR5 antagonist fenobam. As expected, fenobam (10 μM) (in combination with fast transmission blockers and CGP55845) abolished the difference in threshold between genotypes (WT −41.94 ± 0.58 mV, n = 7; KO – 42.53 ± 0.26 mV, n = 8, p = 0.786; Figure 4A).

To further clarify this issue, we estimated the relative contributions of the above-mentioned receptors to neuronal excitability through comparison of the changes in AP threshold by their specific blockers. In the WT neurons, the relative contribution of combining activation of these 5 receptors to AP threshold is about +2 mV as evident by subtracting threshold values obtained with and without all 5 blockers (Figure 4B). This can be interpreted to indicate that the network activity normally maintains the E/I balance via these 5 receptors with slight inhibitory dominance. In contrast, in *Fmr1* KO neurons the net effect of the same 5 receptors is only about +0.06 mV, suggesting that the E/I balance in *Fmr1* KO network

shifts towards increased excitability. We note that addition of any blocker alters not only the individual cells we recorded from, but the entire network excitability; therefore the contribution of a specific receptor to cell excitability can only be determined while all other receptors are blocked. Thus by subtracting threshold values obtained with and without MPEP (or fenobam) in the presence of 4 other blockers, this analysis demonstrates the markedly increased contribution of mGluR5 signaling to AP threshold in *Fmr1* KO compared with WT neurons (MPEP: WT −1.28 mV; KO −4.20 mV; fenobam: WT −1.16 mV; KO −3.69 mV, Figure 4B). In contrast, the contribution of $GABA_B$Rs to AP threshold was very modest in both genotypes (Figure 4B). Taken together, these results indicate that the decreased AP threshold in *Fmr1* KO neurons is caused by the abnormally elevated mGluR5 signaling.

Exaggerated mGluR5 signaling acting via PLC-PKC Pathway Causes Increased Persistent Na^+ Current in *Fmr1* KO neurons

Because our results demonstrate that enhanced I_{NaP} in *Fmr1* KO neurons decreases AP threshold, and that the abnormal AP threshold is also attributed to the elevated mGluR5 activity, we then asked whether the elevated mGluR5 signaling causes enhanced I_{NaP} in *Fmr1* KO neurons. To minimize the network influences from other glutamatergic or GABAergic receptors on I_{NaP}, we measured I_{NaP} in the presence of 4 blockers of NMDA, AMPA, $GABA_A$ and $GABA_B$ receptors. First, we found that I_{NaP} was still significantly larger in the *Fmr1* KO than WT neurons in the presence of these 4 blockers (I_{NaP} at −40 mV: WT −1.40 ± 0.23 pA/pF, n = 7; KO −2.33 ± 0.18 pA/pF, n = 7, p = 0.0092; Figure S3A,B) and was nearly the same as I_{NaP} measured without the blockers (Figure 3D), while the voltage-dependent activation of I_{NaP} was unaffected in both genotypes (Figure S3C). These results support the notion that these four receptors modulate AP threshold through mechanisms other than I_{NaP}. In contrast, when mGluR5 blocker MPEP (10 μM) was combined with the other 4 blockers, it decreased the I_{NaP} in *Fmr1* KO neurons (Figure 4C,H) and, most importantly, MPEP abolished the difference in I_{NaP} between genotypes (with MPEP, at −40 mV: WT −1.20 ± 0.15 pA/pF, n = 6; KO −1.14 ± 0.28 pA/pF, n = 6, p = 0.871; Figure 4C,H). We note that MPEP decreased I_{NaP} predominately in *Fmr1* KO neurons, with negligible effect in WT neurons. These results indicate that elevated mGluR5 signaling leads to enhanced I_{NaP} in *Fmr1* KO neurons.

Rapid normalization of I_{NaP} in *Fmr1* KO neurons by acute inhibition of mGluR5 suggests that the effects of elevated mGluR5 signaling on I_{NaP} are mediated, at least in part, by modulation of Na^+ channel activity. Indeed, pharmacological activation of Group I mGluRs has been shown to modulate activity of Na^+ channels and specifically I_{NaP} (Carlier et al., 2006; D'Ascenzo et al., 2009; Dong and Ennis, 2013) in a PLC-dependent manner (D'Ascenzo et al., 2009). To probe the signaling pathway mediating mGluR5 actions on I_{NaP} in *Fmr1* KO neurons, we examined the effects of disrupting the mGluR5-PLC signaling pathway using a selective PLC inhibitor, edelfosine. Application of edelfosine (1 μM) via the recording pipette (to avoid network effects) completely abolished the differences in I_{NaP} between genotypes (at −40 mV: WT −1.62 ± 0.20 pA/pF, n = 6, KO −1.28 ± 0.21 pA/pF, n = 6, p = 0.3089, Figure 4D,H). Intracellular application of another PLC inhibitor U73122 (1 μM) similarly abolished the difference in I_{NaP} between genotypes (at −40 mV: WT −1.10

± 0.18 pA/pF, n = 6, KO −1.27 ± 0.28 pA/pF, n = 6, p =0.574, Figure 4E,H). PKC is the major downstream effector of PLC activation (Mochly-Rosen et al., 2012) and is a well known modulator of Na^+ channel activity (Li et al., 1993). We therefore further tested if PKC activation downstream of PLC mediates the observed changes in I_{NaP} using two potent and selective PKC inhibitors calphostin C and $PKC_{19–36}$ (a pseudosubstrate peptide inhibitor of PKC). Intracellular application of either calphostin C (10 μM) or $PKC_{19–36}$ (2 μM) via the recording pipette completely abolished the differences in I_{NaP} between genotypes (Figure 4F, G, H) (calphostin C at −40 mV: WT −1.16 ± 0.23 pA/pF, n =6, KO −1.42 ± 0.20 pA/pF, n = 6, p = 0.50199; $PKC_{19–36}$: WT −1.18 ± 0.21 pA/pF, n = 7, KO −1.11 ± 0.11 pA/pF, n = 6, p = 0.8308).

Taken together, our results suggest that an exaggerated activity of mGluR5 acting via PLCPKC signaling pathway enhances I_{NaP} in *Fmr1* KO neurons, which in turn leads to decreased AP threshold and increased neuronal excitability in the EC layer III PCs of *Fmr1* KO mice.

DISCUSSION

Here we demonstrate that PCs in the EC layer III of *Fmr1* KO mice have a decreased AP threshold and increased excitability caused by dysregulation of Na^+ channels. Our results indicate that this Na^+ channel dysregulation is mediated by exaggerated mGluR5-PLC-PKC signaling that markedly increases persistent Na^+ current in *Fmr1* KO neurons. These findings suggest that Na^+ channel dysregulation plays a major role in neuronal hyperexcitability in an FXS mouse model. Our results also reveal an important mechanism by which abnormal mGluR5 signaling causes neuronal hyperexcitability in the absence of FMRP. The finding that inhibition of I_{NaP} eliminates differences in AP threshold between *Fmr1* KO and WT neurons suggests an avenue for development of therapeutic strategies to normalize neuronal hyperexcitability in FXS.

Emerging evidence links hyperexcitability in FXS with dysfunction in a number of ion channels, predominately K^+ channels (Brown et al., 2010; Deng et al., 2013; Gross et al., 2011; Kalmbach et al., 2015; Lee and Jan, 2012; Myrick et al., 2015; Routh et al., 2013; Zhang et al., 2014) and HCN channels (Brager et al., 2012; Zhang et al., 2014). Among the conductances that modulate neuronal excitability, the sub-threshold voltage-dependent conductances are critical to both the membrane excitability state and synaptic integration via regulation of both RMP and AP threshold. I_M, I_h and I_{NaP} are the three major sub-threshold conductances in central neurons that are active and do not inactivate at sub-threshold voltages, and thus play a critical role in setting neuronal excitability (Honigsperger et al., 2015; Yamada-Hanff and Bean, 2013, 2015). However, these three conductances have distinct pattern of voltage dependence: subthreshold depolarization enhances I_M and I_{NaP}, but dampens I_h; in contrast, sub-threshold hyperpolarization dampens I_M and I_{NaP}, but enhances I_h. As a result, these three conductances differentially contribute to regulation of RMP and AP threshold. In agreement with this notion, we found that reduced AP threshold of EC layer III PCs in *Fmr1* KO mice is caused by enhanced 10 I_{NaP}, but not I_M or I_h. We note that our results do not exclude a possibility that in addition to I_{NaP}, I_{NaT} is also altered in *Fmr1* KO neurons. Indeed, the maximal rise speed of AP, a Na^+ channel-dependent

parameter, is increased in *Fmr1* KO neurons ($p = 0.00368$, data not shown), which might indicate a change in I_{NaT}.

Our data further indicate that changes in both I_{NaP} and the AP threshold are mediated by exaggerated mGluR5 signaling in the absence of FMRP. It is well accepted that loss of FMRP causes abnormally elevated mGluR5 activity (Santoro et al., 2012). PLC is a well-defined effector of mGluR5 signaling (Kettunen et al., 2002) and is well known to modulate activity of voltage-gated ion channels and specifically I_{NaP} (D'Ascenzo et al., 2009). The receptor-dependent activation of PLC results in generation of diacylglycerol and IP3. IP3, in turn, triggers the release of calcium from the ER, causing a rise in cytosolic calcium concentration, which then activates PKC (Kettunen et al., 2002). Activation of PKC has been shown to increase neuronal excitability by enhancing I_{NaP} at subthreshold voltages in neocortical neurons (Astman et al., 2006). In addition, activation of mGluR5 by DHPG in WT mice has been shown to upregulate I_{NaP} (Carlier et al., 2006; D'Ascenzo et al., 2009). Our results suggest that the increased I_{NaP} in *Fmr1* KO neurons is caused by exaggerated activity of mGluR5 acting via PLC-PKC pathway. This is a distinct signaling mechanism than the well-established signaling cascade by which abnormal mGluR5 activation impacts local translation in *Fmr1* KO animals (Santoro et al., 2012). While we cannot rule out the possibility that changes in I_{NaP} are mediated in part by altered Na^+ channel expression, our results indicate that the functional regulation of I_{NaP} by mGluR5 is sufficient to account for the changes in AP threshold in *Fmr1* KO neurons. This notion is supported by the findings that either I_{NaP} inhibitors or I_{NaP} opener are sufficient to abolish the differences in AP threshold between genotypes. This is further supported by the observation that in PCs isolated from circuit activity (via blockade of both ionic and metabotropic transmission receptors), the maximal rise speed of AP is no longer different between genotypes ($p = 0.758$, data not shown)—suggesting that in the absence of circuit activity, Na^+ channel properties are similar in *Fmr1* KO and WT animals. Taken together, these results uncover a distinct mechanism by which abnormal mGluR5 signaling causes hyperexcitability in cortical neurons of *Fmr1* KO mice.

Effects of excessive mGluR5 signaling on circuit excitability are reflected in prolongation of cortical UP states in *Fmr1* KO mice (Hays et al., 2011) and our findings point to I_{NaP} as a potential target to alleviate these hyperexcitability defects. Indeed, although the amplitude of I_{NaP} is small relative to the transient Na^+ current, this persistent component is highly functionally significant because it is activated ~10 mV negative to the threshold potential and is characterized by steep voltage dependence at subthreshold potentials, thus providing strongly positive feedback for further depolarization (Bean, 2007; Crill, 1996). These features make neurons with increased I_{NaP} particularly susceptible to hyperexcitability defects leading to seizures (Stafstrom, 2007), a common dysfunction in FXS. Indeed, pro-epileptic conditions have been associated with elevated I_{NaP} (Azouz et al., 1996; Somjen and Muller, 2000), and mutations in Na^+ channels that cause increases in I_{NaP} have been found in patients with epilepsy (Meisler and Kearney, 2005; Vreugdenhil et al., 2004; Rhodes et al., 2005). Moreover, I_{NaP} inhibitors have been effective in treating both partial and generalized tonic-clonic seizures in humans (Stafstrom, 2007). A number of anti-epileptic drugs are I_{NaP} inhibitors and have no effects on transient Na^+ current at therapeutic concentrations (Segal and Douglas, 1997; Spadoni et al., 2002; Taverna et al., 1998). Given

that hyperexcitability-associated phenotypes are common in FXS, our finding that enhanced I_{NaP} has a profound effect on neuronal excitability in EC layer III PCs of *Fmr1* KO mice suggests that it may play an important role in the pathophysiology of FXS. I_{NaP} may thus represent a therapeutic target for treating hyperexcitability defects in FXS.

EXPERIMENTAL PROCEDURES

Animals and slice preparation

Fmr1 KO and WT control mice on FVB background were obtained from The Jackson Laboratory. Slices were prepared as previously described (Deng et al., 2013). All animal procedures were in compliance with the NIH Guide for the Care and Use of Laboratory Animals, and conformed to Washington University Animal Studies Committee guidelines.

Electrophysiology

Whole-cell recordings using a Multiclamp 700B amplifier (Molecular Devices) were made from pyramidal or stellate cells of EC superficial layers. For I_{NaP} recordings, cell capacitance was compensated. Series resistance compensation was enabled with 80–90% correction and 16 μs lag. I_{NaP} was isolated by subtracting current in 1 μM TTX from that before TTX. All recordings were conducted at near-physiological temperature (33–34°C).

Statistical analysis

Data are presented as mean ± SEM. Student's paired or unpaired t test was used for statistical analysis as appropriate; significance was set as $p < 0.05$. The n was number of cells tested.

Supplementary Material

Refer to Web version on PubMed Central for supplementary material.

Acknowledgments

This work was supported in part by a grant R01 NS081972 to VAK from the NINDS. We thank Mrs. Owyoung for her constructive comments.

REFERENCES

Astman N, Gutnick MJ, Fleidervish IA. Persistent sodium current in layer 5 neocortical neurons is primarily generated in the proximal axon. J Neurosci. 2006; 26:3465–3473. [PubMed: 16571753]

Azouz R, Jensen MS, Yaari Y. Ionic basis of spike after-depolarization and burst generation in adult rat hippocampal CA1 pyramidal cells. J Physiol. 1996; 492(Pt 1):211–223. [PubMed: 8730596]

Bean BP. The action potential in mammalian central neurons. Nat Rev Neurosci. 2007; 8:451–465. [PubMed: 17514198]

Bear MF, Huber KM, Warren ST. The mGluR theory of fragile X mental retardation. Trends Neurosci. 2004; 27:370–377. [PubMed: 15219735]

Brager DH, Akhavan AR, Johnston D. Impaired dendritic expression and plasticity of h-channels in the fmr1(-/y) mouse model of fragile X syndrome. Cell Rep. 2012; 1:225–233. [PubMed: 22662315]

Brown MR, Kronengold J, Gazula VR, Chen Y, Strumbos JG, Sigworth FJ, Navaratnam D, Kaczmarek LK. Fragile X mental retardation protein controls gating of the sodium-activated potassium channel Slack. Nat Neurosci. 2010; 13:819–821. [PubMed: 20512134]

Carlier E, Sourdet V, Boudkkazi S, Deglise P, Ankri N, Fronzaroli-Molinieres L, Debanne D. Metabotropic glutamate receptor subtype 1 regulates sodium currents in rat neocortical pyramidal neurons. J Physiol. 2006; 577:141–154. [PubMed: 16931548]

Carter BC, Bean BP. Sodium entry during action potentials of mammalian neurons: incomplete inactivation and reduced metabolic efficiency in fast-spiking neurons. Neuron. 2009; 64:898–909. [PubMed: 20064395]

Chatzikonstantinou A. Epilepsy and the hippocampus. Front Neurol Neurosci. 2014; 34:121–142. [PubMed: 24777136]

Contractor A, Klyachko VA, Portera-Cailliau C. Altered Neuronal and Circuit Excitability in Fragile X Syndrome. Neuron. 2015; 87:699–715. [PubMed: 26291156]

Crill WE. Persistent sodium current in mammalian central neurons. Annu Rev Physiol. 1996; 58:349–362. [PubMed: 8815799]

D'Ascenzo M, Podda MV, Fellin T, Azzena GB, Haydon P, Grassi C. Activation of mGluR5 induces spike afterdepolarization and enhanced excitability in medium spiny neurons of the nucleus accumbens by modulating persistent Na+ currents. J Physiol. 2009; 587:3233–3250. [PubMed: 19433572]

Deng PY, Rotman Z, Blundon JA, Cho Y, Cui J, Cavalli V, Zakharenko SS, Klyachko VA. FMRP regulates neurotransmitter release and synaptic information transmission by modulating action potential duration via BK channels. Neuron. 2013; 77:696–711. [PubMed: 23439122]

Gibson JR, Bartley AF, Hays SA, Huber KM. Imbalance of neocortical excitation and inhibition and altered UP states reflect network hyperexcitability in the mouse model of fragile X syndrome. J Neurophysiol. 2008; 100:2615–2626. [PubMed: 18784272]

Gross C, Yao X, Pong DL, Jeromin A, Bassell GJ. Fragile X mental retardation protein regulates protein expression and mRNA translation of the potassium channel Kv4.2. J Neurosci. 2011; 31:5693–5698. [PubMed: 21490210]

Hammarstrom AK, Gage PW. Inhibition of oxidative metabolism increases persistent sodium current in rat CA1 hippocampal neurons. J Physiol. 1998; 510:735–741. [PubMed: 9660889]

Hays SA, Huber KM, Gibson JR. Altered neocortical rhythmic activity states in Fmr1 KO mice are due to enhanced mGluR5 signaling and involve changes in excitatory circuitry. J Neurosci. 2011; 31:14223–14234. [PubMed: 21976507]

Honigsperger C, Marosi M, Murphy R, Storm JF. Dorsoventral differences in Kv7/M-current and its impact on resonance, temporal summation and excitability in rat hippocampal pyramidal cells. J Physiol. 2015; 593:1551–1580. [PubMed: 25656084]

Kalmbach BE, Johnston D, Brager DH. Cell-Type Specific Channelopathies in the Prefrontal Cortex of the fmr1-/y Mouse Model of Fragile X Syndrome. eNeuro 2. 2015

Kettunen P, Krieger P, Hess D, El Manira A. Signaling mechanisms of metabotropic glutamate receptor 5 subtype and its endogenous role in a locomotor network. J Neurosci. 2002; 22:1868–1873. [PubMed: 11880516]

Lee HY, Jan LY. Fragile X syndrome: mechanistic insights and therapeutic avenues regarding the role of potassium channels. Curr Opin Neurobiol. 2012; 22:887–894. [PubMed: 22483378]

Li M, West JW, Numann R, Murphy BJ, Scheuer T, Catterall WA. Convergent regulation of sodium channels by protein kinase C and cAMP-dependent protein kinase. Science. 1993; 261:1439–1442. [PubMed: 8396273]

Meisler MH, Kearney JA. Sodium channel mutations in epilepsy and other neurological disorders. J Clin Invest. 2005; 115:2010–2017. [PubMed: 16075041]

Myrick LK, Deng PY, Hashimoto H, Oh YM, Cho Y, Poidevin MJ, Suhl JA, Visootsak J, Cavalli V, Jin P, et al. Independent role for presynaptic FMRP revealed by an FMR1 missense mutation associated with intellectual disability and seizures. Proc Natl Acad Sci U S A. 2015; 112:949–956. [PubMed: 25561520]

Pacey LK, Heximer SP, Hampson DR. Increased GABA(B) receptor-mediated signaling reduces the susceptibility of fragile X knockout mice to audiogenic seizures. Mol Pharmacol. 2009; 76:18–24. [PubMed: 19351745]

Platkiewicz J, Brette R. A threshold equation for action potential initiation. PLoS Comput Biol. 2010; 6:e1000850. [PubMed: 20628619]

Rhodes TH, Vanoye CG, Ohmori I, Ogiwara I, Yamakawa K, George AL Jr. Sodium channel dysfunction in intractable childhood epilepsy with generalized tonic-clonic seizures. J Physiol. 2005; 569:433–445. [PubMed: 16210358]

Routh BN, Johnston D, Brager DH. Loss of functional A-type potassium channels in the dendrites of CA1 pyramidal neurons from a mouse model of fragile X syndrome. J Neurosci. 2013; 33:19442–19450. [PubMed: 24336711]

Santoro MR, Bray SM, Warren ST. Molecular mechanisms of fragile X syndrome: a twenty-year perspective. Annu Rev Pathol. 2012; 7:219–245. [PubMed: 22017584]

Segal MM, Douglas AF. Late sodium channel openings underlying epileptiform activity are preferentially diminished by the anticonvulsant phenytoin. J Neurophysiol. 1997; 77:3021–3034. [PubMed: 9212254]

Somjen GG, Muller M. Potassium-induced enhancement of persistent inward current in hippocampal neurons in isolation and in tissue slices. Brain Res. 2000; 885:102–110. [PubMed: 11121535]

Spadoni F, Hainsworth AH, Mercuri NB, Caputi L, Martella G, Lavaroni F, Bernardi G, Stefani A. Lamotrigine derivatives and riluzole inhibit INa,P in cortical neurons. Neuroreport. 2002; 13:1167–1170. [PubMed: 12151762]

Stafstrom CE. Persistent sodium current and its role in epilepsy. Epilepsy Curr. 2007; 7:15–22. [PubMed: 17304346]

Tang AH, Alger BE. Homer protein-metabotropic glutamate receptor binding regulates endocannabinoid signaling and affects hyperexcitability in a mouse model of fragile X syndrome. J Neurosci. 2015; 35:3938–3945. [PubMed: 25740522]

Taverna S, Mantegazza M, Franceschetti S, Avanzini G. Valproate selectively reduces the persistent fraction of Na+ current in neocortical neurons. Epilepsy Res. 1998; 32:304–308. [PubMed: 9761329]

Urbani A, Belluzzi O. Riluzole inhibits the persistent sodium current in mammalian CNS neurons. Eur J Neurosci. 2000; 12:3567–3574. [PubMed: 11029626]

Vreugdenhil M, Hoogland G, van Veelen CW, Wadman WJ. Persistent sodium current in subicular neurons isolated from patients with temporal lobe epilepsy. Eur J Neurosci. 2004; 19:2769–2778. [PubMed: 15147310]

Wahlstrom-Helgren S, Klyachko VA. $GABA_B$ Receptor-Mediated Feed-Forward Circuit Dysfunction in the Mouse Model of Fragile X Syndrome. J Physiol. 2015; 593:5009–5024. [PubMed: 26282581]

Yamada-Hanff J, Bean BP. Persistent sodium current drives conditional pacemaking in CA1 pyramidal neurons under muscarinic stimulation. J Neurosci. 2013; 33:15011–15021. [PubMed: 24048831]

Yamada-Hanff J, Bean BP. Activation of Ih and TTX-sensitive sodium current at subthreshold voltages during CA1 pyramidal neuron firing. J Neurophysiol. 2015; 114:2376–2389. [PubMed: 26289465]

Zhang Y, Bonnan A, et al. Dendritic channelopathies contribute to neocortical and sensory hyperexcitability in Fmr1(-/y) mice. Nat Neurosci. 2014; 17:1701–1709. [PubMed: 25383903]

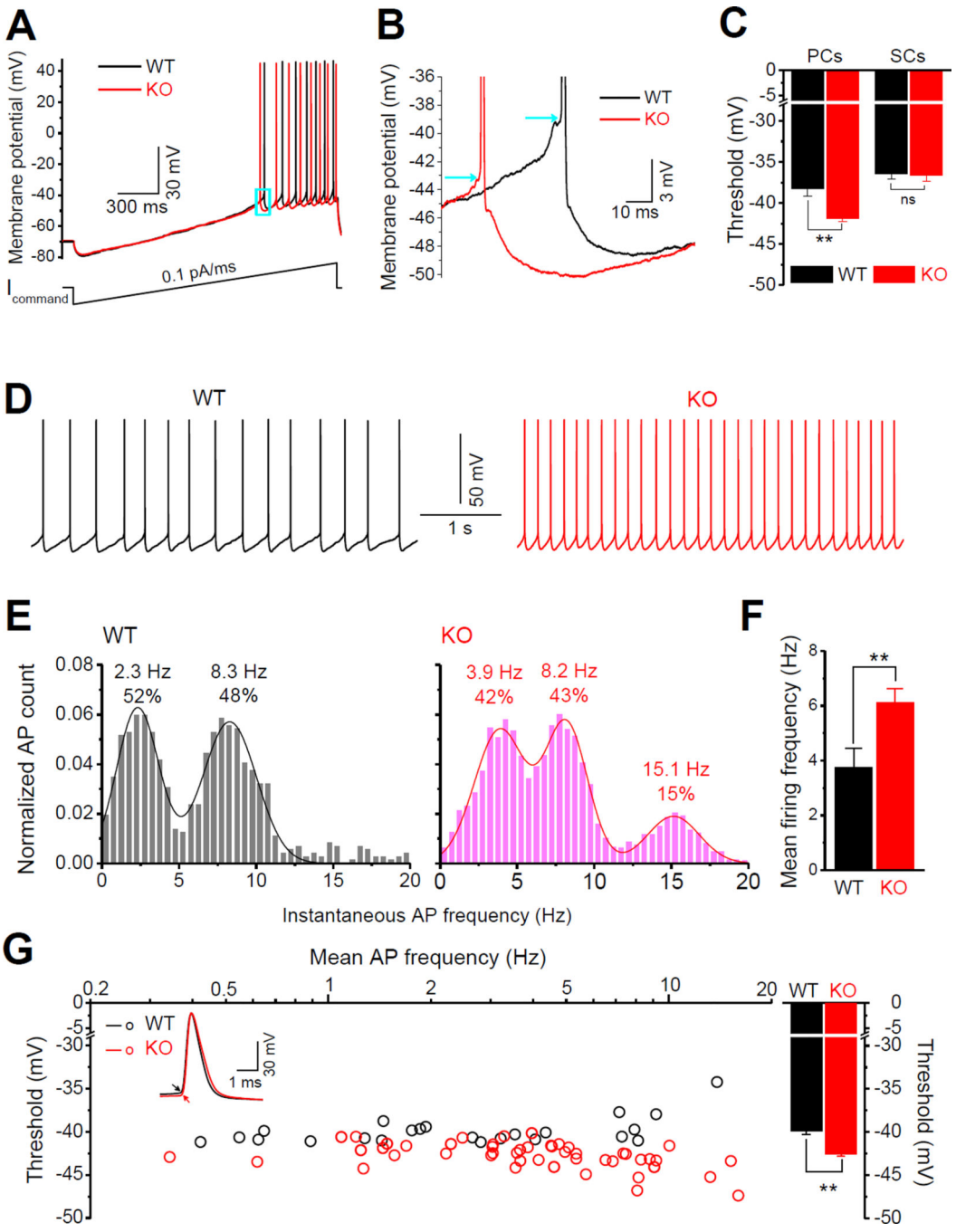

Figure 1. Increased Neuronal Excitability in the EC Layer III PCs of *Fmr1* KO Mice

(**A**) Determination of AP threshold. APs were evoked by a ramp current injection (~0.1pA/ms, lower trace). Representative AP traces from EC layer III PCs are shown (upper traces). Only the 1st AP was used to estimate AP threshold (box area).

(**B**) Enlargement of boxed area in (**A**) showing a hyperpolarizing shift of threshold voltage in *Fmr1* KO neuron. Arrows denote the thresholds in WT and *Fmr1* KO neurons.

(**C**) Decreased threshold voltage was found in the PCs, but not stellate cells (SCs), in the EC superficial layers.

(**D**) Sample traces of spontaneous APs recorded at −51 mV in WT and *Fmr1* KO neurons.
(**E**) AP frequency distribution. A bin size of 0.5 Hz was used to calculate AP firing frequency distribution from a 20-s long trace per cell. The number of APs within a bin was divided by the total number of APs for pooling the data from all tested cells. Insert numbers denote the peak frequency and percentile estimated from Gaussian fits.
(**F**) Mean AP firing frequency in *Fmr1* KO and WT EC layer III PCs, data averaged from (**E**).
(**G**) Threshold estimates for spontaneous APs. Each point represents an averaged AP threshold in one cell (from all APs in a 20s-long trace in each cell). Insert AP traces show a hyperpolarizing shift of threshold in *Fmr1* KO neurons (arrows). Bar graph shows mean thresholds for all cells.
** $p < 0.01$; ns, not significant. All data are mean ± SEM.

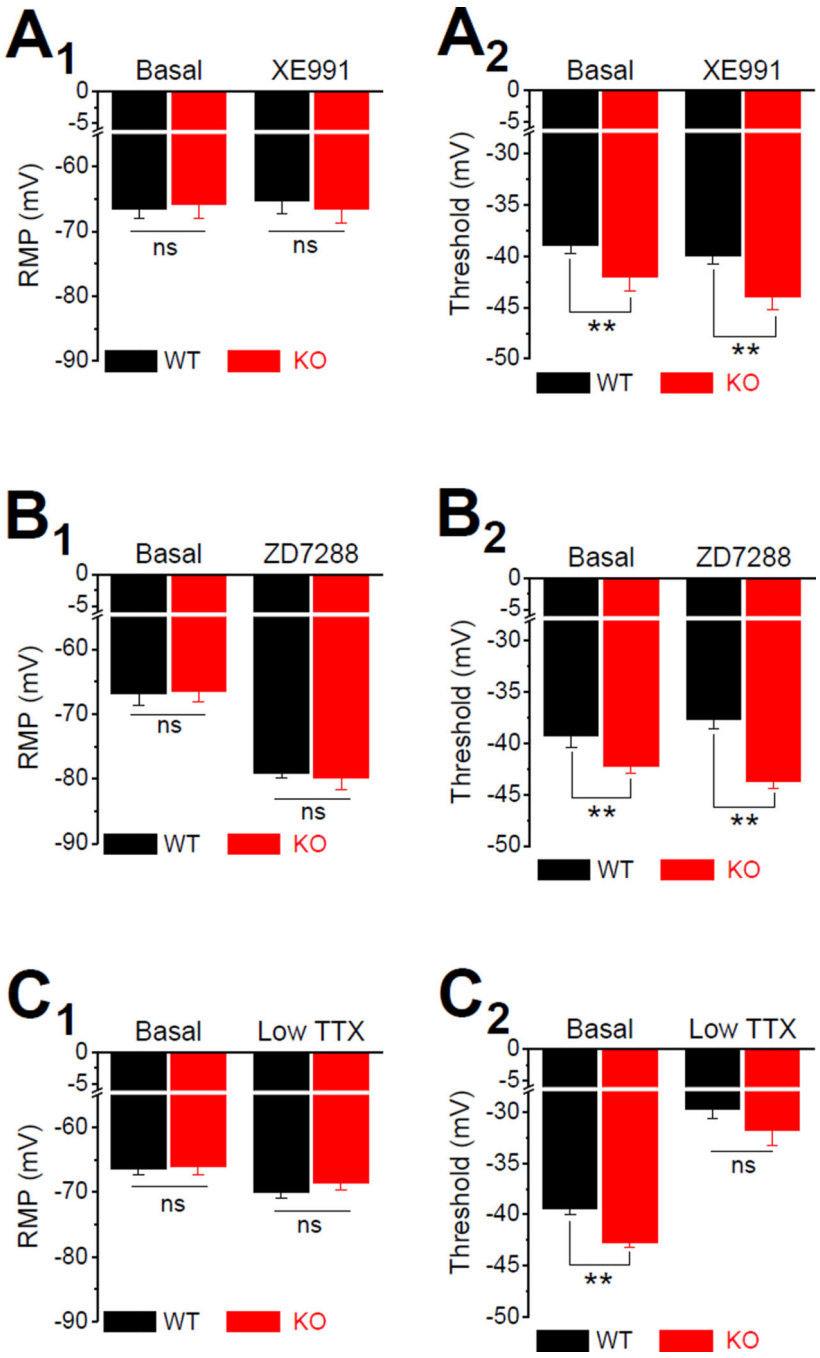

Figure 2. Abnormal Persistent Na^+ current in EC Layer III PCs of *Fmr1* KO Mice

(**A**) Effect of Kv7 channel inhibitor XE991 on RMP (**A_1**) and AP threshold (**A_2**).

(**B**) Same as (**A**) for HCN channel blocker, ZD7288.

(**C**) Same as (**A**) for I_{NaP} blocker, 20 nM TTX.

* $p < 0.05$, ** $p < 0.01$. All data are mean ± SEM.

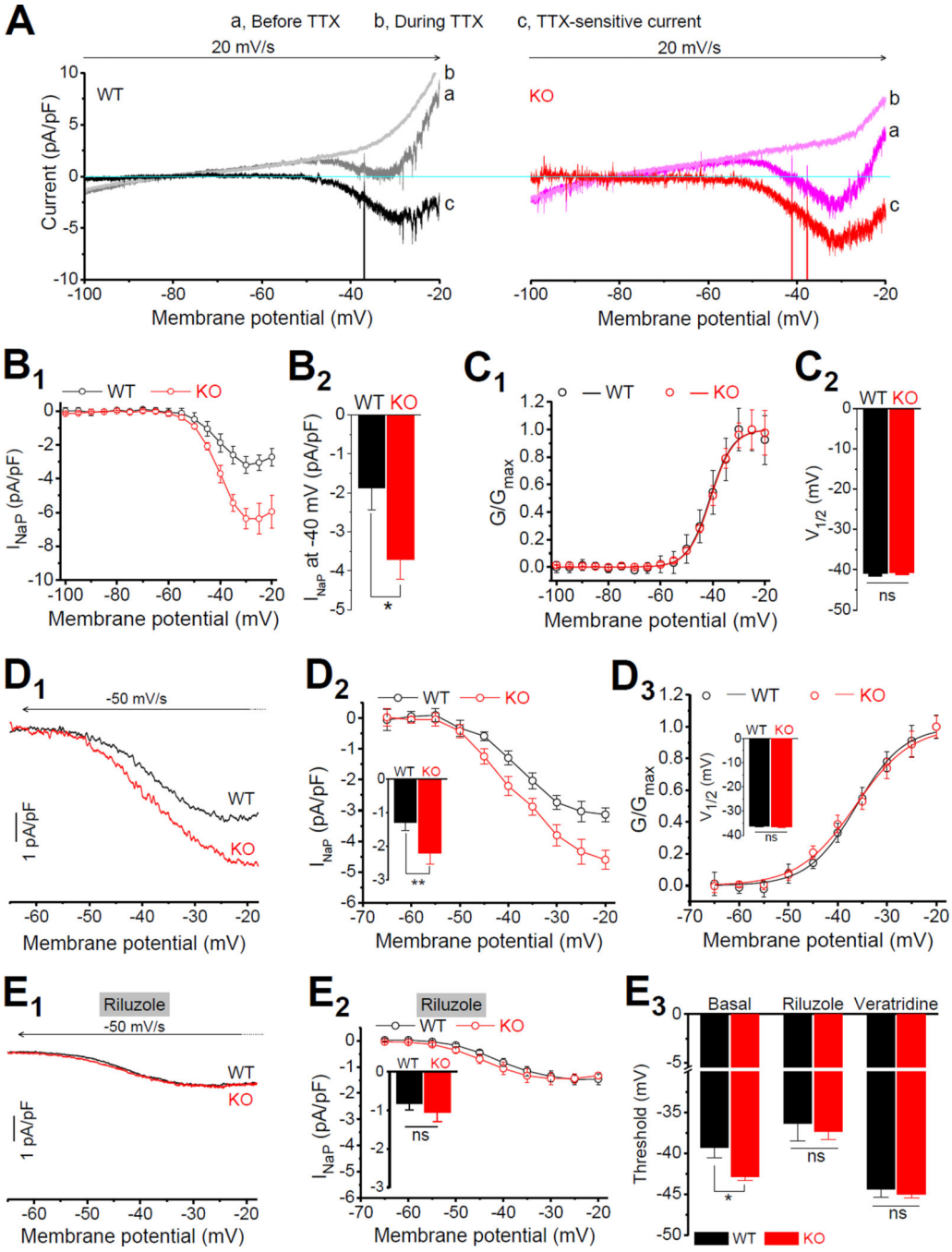

Figure 3. Enhanced Persistent Na^+ Current Underlies AP Threshold Changes in *Fmr1* KO neurons

(**A**) I_{NaP} evoked by a depolarizing voltage ramp (−100 to −20 mV, 20 mV/s) before (*traces a*) and during (*traces b*) application of TTX. TTX-sensitive current (*traces c*) was obtained by subtraction. Note that the large escaped AP currents were truncated to emphasize the I_{NaP}.

(**B**) I-V curves (**B_1**) were constructed from the ramp evoked I_{NaP} (mean current value over 0.01 mV intervals from averages of 4–5 trials for each cell to approximating quasi-steady

state current). Currents were normalized to corresponding cell capacitance for better comparison. (**B_2**) I_{NaP} at −40 mV was significantly large in *Fmr1* KO neurons. (**C**) Voltage-dependent activation curve of I_{NaP} (**C_1**). Data fitted by Boltzmann function. Summarized data of half activation voltage $V_{1/2}$ (**C_2**). (**D**) I_{NaP} evoked by a repolarizing ramp (**D_1**, +30 to −65 mV, −50 mV/s). For better comparison with (**A**), the traces are presented in the same direction as in (**A**) in a −65 to −20 mV range. Arrow indicates the time direction. (**D_2**) The difference of I-V curves between WT and *Fmr1* KO neurons. *Insert*: I_{NaP} at −40 mV. (**D_3**) The voltage-dependent activation of I_{NaP} in *Fmr1* KO and WT neurons. *Insert*: $V_{1/2}$ of I_{NaP} activation. (**E**) Effects of I_{NaP} inhibitor riluzole on the I_{NaP} and AP threshold in *Fmr1* KO and WT neurons. (**E_1**) Sample I_{NaP} traces. (**E_2**) I-V curves. *Insert*, I_{NaP} at −40 mV. (**E_3**) Effects of I_{NaP} inhibitor riluzole and I_{NaP} opener veratridine on AP threshold.
* $p < 0.05$; ** $p < 0.01$; ns, not significant. All data are mean ± SEM.

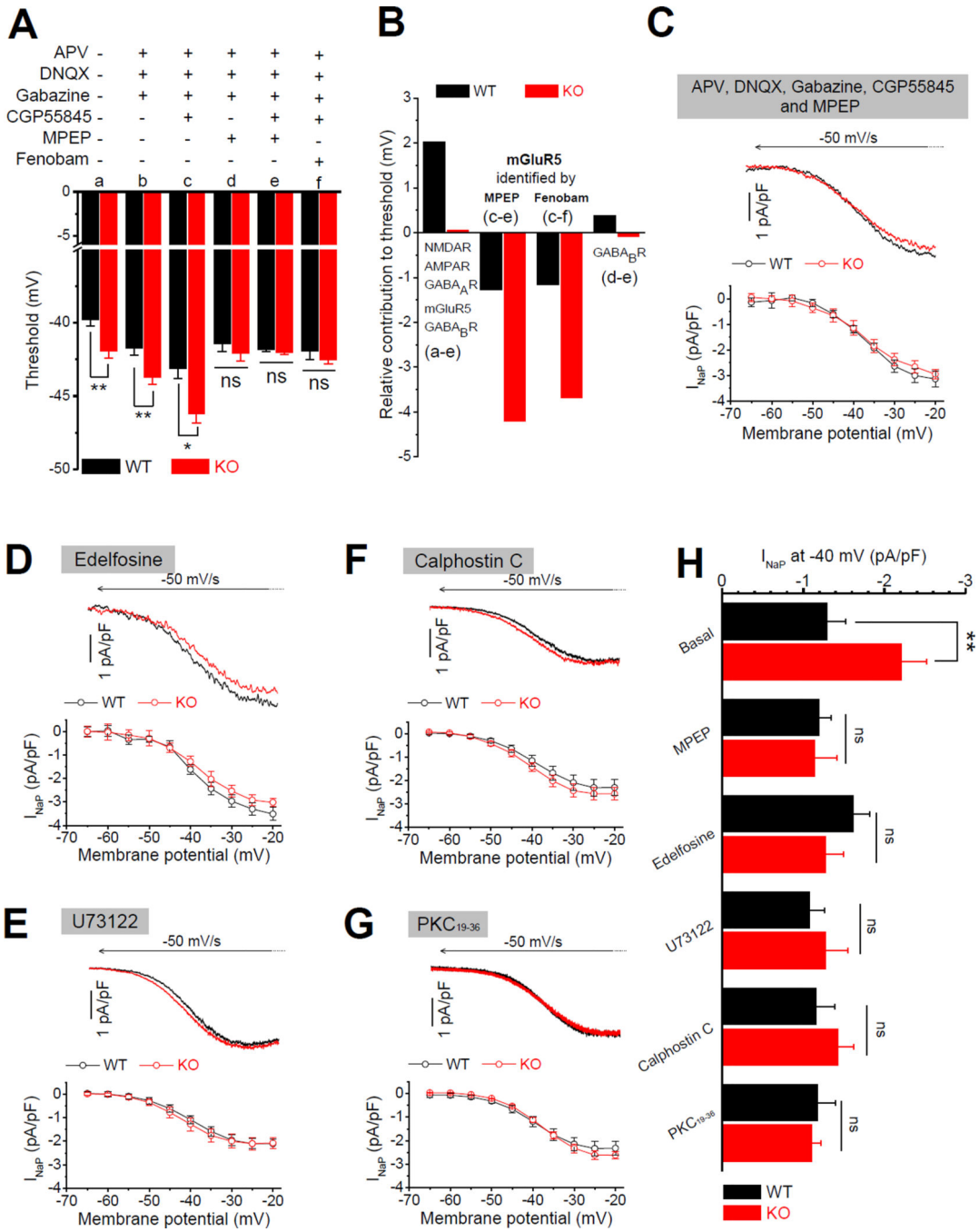

Figure 4. Exaggerated mGluR5-PKC-PLC Signaling Causes Enhanced Persistent Na^+ Current in *Fmr1* KO Neurons

(**A**) Effects of various combinations of blockers on AP threshold.

(**B**) Estimates for receptor contributions to cell excitability from (**A**).

(**C**) Sample I_{NaP} traces (*upper panel*) and summarized data (*lower panel*) for I_{NaP} measured in presence of mGluR5 inhibitor MPEP in combination with 4 other blockers (against NMDA, AMPA, $GABA_A$ and $GABA_B$ receptors).

(**D**) Same as (**C**) for I_{NaP} measured with intracellular application of selective PLC inhibitor edelfosine.
(**E**) Same as (**C**) for I_{NaP} measured with intracellular application of PLC inhibitor U73122.
(**F**) Same as (**C**) for I_{NaP} measured with intracellular application of PKC inhibitor calphostin C.
(**G**) Same as (**C**) for I_{NaP} measured with intracellular application of PKC inhibitor $PKC_{19–36}$.
(**H**) I_{NaP} values at −40 mV summarized from (**C-G**).
* $p < 0.05$; ** $p < 0.01$; ns, not significant. All data are mean ± SEM.